Genetically encoded FRET sensors to monitor intracellular Zn2+ homeostasis

Jan L. Vinkenborg[1], Tamara J. Nicolson[2], Elisa A. Bellomo[2], Melissa S. Koay[1], Guy A. Rutter[2]*, and Maarten Merkx[1]*

[1] Laboratory of Chemical Biology, Department of Biomedical Engineering, Eindhoven University of Technology, Den Dolech 2, 5612AZ Eindhoven, The Netherlands.

[2] Section of Cell Biology, Division of Medicine, Imperial College London, Exhibition Road, South Kensington, SW7 2AZ, London, U.K.

*Correspondence should be addressed to G.A.R g.rutter@imperial.ac.uk or M.M. m.merkx@tue.nl

Abstract

Genetically-encoded Förster Resonance Energy Transfer (FRET)-based sensors were developed that display a large ratiometric change upon Zn^{2+} binding, have affinities that span the pico- to nanomolar range, and can readily be targeted to subcellular organelles. Using this sensor toolbox we show that cytosolic Zn^{2+} is buffered at 400 pM in pancreatic β-cells, while substantially higher Zn^{2+} concentrations are found in insulin-containing secretory vesicles.

Zinc plays a critical role in many fundamental cellular processes, acting as a Lewis acid catalyst in numerous enzymes, having a structural function in DNA binding proteins and acting as a modulator in neurotransmission[1-3]. At the same time, low nanomolar concentrations of free Zn^{2+} can be cytotoxic, rendering zinc homeostasis a delicate balance that is not well understood. While synthetic fluorescent sensors have been used to monitor zinc fluctuations in live cells[2,4], they typically lack control over subcellular localization and often have insufficient affinity to detect the extremely low free Zn^{2+} concentrations. Genetically encoded FRET-based sensor proteins can be used to overcome these limitations[5,6], but their application for imaging transition metal homeostasis has thus far remained underdeveloped.

The FRET sensors reported here are based on a previously developed Zn^{2+} sensor that showed high Zn^{2+} affinity (K_d = 140 fM), but suffered from a small change in emission ratio (15%)[7]. This CALWY sensor consists of two metal binding domains (Atox1 and domain 4 of ATP7B (WD4)) linked via a long flexible linker, with each domain providing two cysteines to form a single tetrahedral zinc binding pocket (Figure 1a). First, we replaced the ECFP and EYFP domains by cerulean and citrine to improve brightness and reduce pH sensitivity of the fluorophores, respectively. Next, the ratiometric response was improved considerably by introduction of mutations (S208F, V224L) on the surface of both fluorescent domains that are known to promote intramolecular complex formation (Figure 1a-d)[8]. As a result, this sensor (eCALWY-1) displays efficient energy transfer in the absence of Zn^{2+}, but shows a large, 2.4-fold decrease in emission ratio upon Zn^{2+} binding (Figure 1d,e). The Zn^{2+} affinity of eCALWY-1 (K_d=2 pM at pH=7.1) was only 10-fold lower than that of the CALWY

sensor, showing that the interaction between the fluorescent domains was easily disrupted by zinc binding. Mutation of one of the zinc-binding cysteines within the WD4 domain (C416S) attenuated the Zn^{2+} affinity 300-fold, yielding eCALWY-4 with a K_d of 600 pM. Importantly, this mutation also abrogated the binding of Cu^{+}, which was shown to induce an interaction between the metal binding domains in eCALWY-1 (Supporting Figure S4). Further fine-tuning of the Zn^{2+} affinity was achieved by shortening the linker between the metal binding domains, yielding a series of sensors (eCALWY1-6) that span the picomolar to nanomolar ranges and display at least a 2-fold ratiometric change upon zinc binding (Figure 1e).

Next we tested the performance of the eCALWY sensors to monitor free cytosolic Zn^{2+} levels using pancreatic β-cells (INS-1(832/13)), a cell-type known to contain high zinc levels in granules specialized in insulin storage[9,10]. All sensors displayed homogeneous expression throughout the cytosol of the cells. A large increase in emission ratio was observed in cells expressing eCALWY-1 after addition of the membrane permeable zinc chelator N,N,N',N'-tetrakis-(2-pyridylmethyl)-ethylenediamine (TPEN), indicative of a decrease in cytosolic zinc (Figure 2a,b). Subsequent perifusion with 5 μM of the zinc ionophore pyrithione had little effect, but together with 100 μM $ZnCl_2$ the ratio rapidly returned to the starting level. Addition of TPEN or Zn^{2+}/pyrithione did not affect the emission ratio of a non-binding sensor variant (Supporting Figure S5). Moreover, a consistent trend was observed for the emission ratio at the start of the experiment, changing from a fully saturated level for eCALWY-1 to nearly unsaturated for eCALWY-6 (Figure 2b-g). The sensor occupancy was calculated using equation (1), in which R_{max} and R_{min} are the steady-state ratios obtained after TPEN and zinc/pyrithione

addition, respectively, and R_{start} is the ratio at the start of the experiment. A plot of the sensor occupancy as a function of its K_d shows a clear sigmoidal shape, that is best described by assuming a free Zn^{2+} concentration of 400 pM (Figure 2h). Interestingly, repeating these experiments in HEK293 cells showed very similar responses (Supporting Figures S7-8, Video S1), suggesting that the 400 pM level may be invariant among different cell lines. In fact, similar values have been reported using synthetic dyes in more indirect measurements on cell populations with Fluozin-3 in human colon cancer HT29 (~600pM)[11] and in fibroblastic L(TK)$^-$ cells with Zinbo-5 (~1000 pM)[12]. Previous studies that tried to estimate free cytosolic Zn^{2+} concentrations using protein-based sensors did not use internal calibration and/or were done outside the sensors' detection range, resulting in either very high (180 nM) or very low (5 pM) numbers[5,6].

$$Occupancy = \frac{R_{\max} - R_{start}}{R_{\max} - R_{\min}} \cdot 100\% \qquad (1)$$

The fact that the occupancies of the entire sensor series can be described by a single concentration of free Zn^{2+} is important, because it implies that the intracellular free Zn^{2+} concentration is strongly buffered and not perturbed significantly by the presence of low μM concentrations of the sensors. To further test this buffering capacity, INS-1(832/13) β-cells expressing eCALWY-4 were cultured overnight in media containing either 100 μM EDTA or a Zn^{2+}-buffer providing 5 μM of free Zn^{2+}. Cells that were cultured in the presence of 100 μM EDTA showed free cytosolic Zn^{2+} concentrations that were similar to cells grown in normal medium, but nanomolar or higher free Zn^{2+} levels were observed in cells cultured in the presence of excess Zn^{2+} (Figure 2i-j). Strikingly, when the latter cells were perifused with buffer containing 100 μM EDTA, cytosolic zinc

levels rapidly decreased to ~400 pM, showing that these cells efficiently restore their intracellular Zn^{2+} levels once excess zinc is removed (Figure 2i-j). No significant decrease in cytosolic zinc was observed for normally cultured cells after perifusion with 100 μM EDTA.

To verify that the cytosolic environment does not affect the sensor K_d, we calibrated the eCALWY-4 sensor *in situ* by perifusion of cells treated with α-toxin using buffers containing different free zinc concentrations. The *in situ* determined K_d confirmed that the intracellular conditions are only weakly affecting the zinc affinity (Supporting Figure S9). Specificity over biologically relevant Ca^{2+} levels could be demonstrated by depolarizing INS-1(832/13) cells with KCl to elicit Ca^{2+} influx. Despite a clear increase in cytosolic Ca^{2+} to 1 μM, no change in the emission was observed in cells expressing eCALWY-5 (Supporting Figure S10).

Since control over intracellular localization is a key advantage of genetically encoded sensors, we next targeted the eCALWY sensors to the insulin granules of INS-1(832/13) cells via fusion to the C-terminus of vesicle targeted membrane protein 2 (VAMP2)[13]. As we anticipated higher free zinc concentrations in these vesicles[9], we also employed a low affinity Zn^{2+}-sensor (eZinCh; K_d=1μM at pH=7.1 and 250 μM at pH=6.0, Supporting Figure S11). eZinCh displays a 4-fold increase in emission ratio upon zinc binding and is similar to the previously reported ZinCh[14], but contains cerulean and citrine as fluorescent domains. Colocalization studies with a granule-localised neuropeptideY-mCherry fusion protein showed that VAMP2-eCALWY-1, VAMP2-eCALWY-6 and VAMP2-eZinCh were indeed exclusively localized in insulin-containing granules (Figure 3a; Supporting Figure S12). The low emission ratios observed for the

eCALWY variants prior to stimulation suggests saturation with Zn^{2+} (Figure 3b), while eZinCh appears to be empty. No changes in emission ratio could be induced using either TPEN or Zn^{2+}/pyrithione for VAMP2-eCALWY-1 and VAMP2-eZinCh, probably reflecting an inability of these agents to induce sufficient changes in the intravesicular free Zn^{2+} concentration (Supporting Figure S13). However, robust and reversible ratiometric changes were observed for VAMP2-eZinCh upon addition of monensin (Figure 3b; supplementary video S2). This Na^+/H^+ exchanger increases the pH of granules from ~ pH 6.0 to pH 7.1, simultaneously increasing the affinity of eZinCh and inducing Zn^{2+} release from the insulin-Zn^{2+} complex. Changes due to the pH sensitivity of the fluorescent domains could be excluded since monensin addition did not induce similar ratiometric changes for a non-binding variant of eZinCh (eZinCh-NB) or any of the eCALWY variants. These results imply that the VAMP2-eCALWY sensors are saturated with Zn^{2+} under normal conditions (K_d=0.5 μM at pH 6.0 for VAMP2-eCALWY-6, Supporting Figure S14) and that VAMP2-eZinCh is mostly Zn^{2+}-free, thus suggesting that the free Zn^{2+} concentration in these vesicles resides between 1 and 100 μM.

In conclusion, we have developed a new generation of Zn^{2+} probes that can be used to image low concentrations of free Zn^{2+} dynamically and in real time in living cells. Cytosolic levels of free Zn^{2+} were found to be buffered at ~400 pM, which coincides with the Zn^{2+}-buffering capacity of metallothioneins[15]. Intriguingly, cytosolic Zn^{2+} concentrations are maintained at a level that is sufficient to fully saturate native Zn^{2+} proteins (which typically show K_d's of 1-10 pM), but approximately 10-fold below the low nM concentrations that have been reported to inhibit several cytosolic proteins[3]. We

also demonstrate that these probes can be targeted to subcellular organelles, including secretory granules. This ability to study Zn^{2+} homeostasis on a (sub)cellular level in real time provides exciting new opportunities to enhance our understanding of the role of zinc homeostasis in health and disease.

Figure legends

Figure 1: **Design and properties of eCALWY-1, a genetically-encoded Zn^{2+} sensor based on conformational switching.** Schematic representation of the CALWY (a) and eCALWY-1 (b) sensor design. ATOX1 and the fourth domain of ATP7B (WD4) are used as metal binding domains. The CALWY sensor suffers from a small FRET change due the presence of a distribution of conformations in the Zn^{2+}-free state, whose average energy transfer efficiency is only slightly higher than the amount of energy transfer in the Zn^{2+}-bound state. Emission spectra of CALWY (c) and eCALWY-1 (d) before (black line) and after (red line) addition of 0.9 mM Zn^{2+} in 1 mM HEDTA (c) or EGTA (d). Zn^{2+} titrations of the eCALWY variants (e), showing the ratio of citrine and cerulean emission (R527/475) as a function of Zn^{2+} concentration using 420 nm excitation. The solid lines depict fits assuming single binding events and corresponding K_d's are listed for each variant. Measurements were performed using ~ 1 μM protein in 150 mM Hepes, 100 mM NaCl, 10% (v/v) glycerol, 1 mM DTT pH 7.1 at 20 ºC. Free zinc concentrations from the picomolar to the nanomolar range were obtained by using different chelators such as EDTA as buffering system (Supporting Table S2).

Figure 2: **Determination of cytosolic free Zn^{2+} concentration in INS-1(832/13) cells using a toolbox of eCALWY variants.** (a) False colored spinning disc confocal microscopy images of INS-1(832/13) cells expressing eCALWY-4 after 60, 380, and 440 s of the experiment described in (b-f). (b-f) Responses of single INS-1(832/13) cells expressing the different eCALWY variants to perifusion with Krebs-Hepes/Bicarbonate (KB) buffer containing 50 μM TPEN (1), 5 μM pyrithione (2) or 5 μM pyrithione/100

μM Zn^{2+} (3) using epifluorescence microscopy. KB comprised of 140 mM NaCl, 3.6 mM KCl, 0.5 mM NaH_2PO_4, 0.5 mM $MgSO_4$, 1.5 mM $CaCl_2$, 10 mM Hepes, 2 mM $NaHCO_3$ and 3 mM glucose, pH 7.4. (h) Sensor occupancy in INS-1(832/13) cells as a function of the sensor K_d for different eCALWY variants as determined from the traces in Supplementary Figure S7 using equation (1); error bars indicate the standard deviation. The dashed lines depict the expected responses assuming free zinc concentrations of 50, 100, 200, 400 (solid line), 800, 1600 and 3200 pM, respectively. (i) Effect of culturing conditions on the ratiometric response of eCALWY-4 expressed in INS-1(832/13) cells. Cells were cultured deprived of zinc (100 μM EDTA), under normal conditions, or in excess zinc (5 μM of buffered Zn^{2+}) for 20 h. During imaging, cells were perifused with KB-plus (KBP), to which 100 μM EDTA (1), 50 μM TPEN (2), or 5 μM pyrithione/100 μM $ZnCl_2$ was added. KBP is similar to KB, but contains 25 mM $NaHCO_3$ instead of 2 mM to prevent cytosolic pH changes from affecting fluorescence. (j) Bar diagram displaying the occupancy of eCALWY-4 in the experiments depicted above (Figure 2i) at the start of perifusion with KB that mimics culturing conditions, and after 10 minutes of perifusion with KB containing 100 μM EDTA. Error bars indicate the standard deviation.

Figure 3: **Subcellular targeting of Zn^{2+} probes to insulin storing granules.** (a) CLSM images of INS-1(832/13) cells co-transfected with VAMP2-eCALWY-1 and neuropeptideY-mCherry. The VAMP2-eCALWY-1 emission was obtained using excitation at 440 nm, while excitation at 595 nm was used to image NPY-mCherry. The scale bar represents 10 μm. (b) Ratiometric response of INS-1(832/13) cells expressing different VAMP2-eCALWY variants, VAMP2-eZinCh and VAMP2-eZinCh-NB to perifusion with 10 μM monensin (1), followed by KBP buffer (2).

Note: Supplementary information is available.

Acknowledgements

We thank S.M.J. van Duijnhoven for the expression and characterization of eZinCh, Dr. A. McDonald for assisting in the spinning disc confocal microscopy experiments, Dr. A. Tarasov for setting up the α-toxin incubation, Prof. H. Bayley (University of Oxford) for kindly providing the α-toxin and Dr Chris Newgard (Duke University) for the provision of INS-1(832/13) cells. We also thank Dr L. Klomp and P. van den Berghe (University Medical Center Utrecht) and Prof. E.W. Meijer for their support at various stages of this research. MM and MSK acknowledge support by the Human Frontier of Science Program (HPSF Young Investigator Grant, (RGY)0068-2006). GAR thanks the National Institutes of Health for Project grant RO1 DK071962-01, the Wellcome Trust for Programme grants 067081/Z/02/Z and 081958/Z/07/Z, the MRC (UK) for Research Grant G0401641, and the EU FP6 ("SaveBeta" consortium grant). TJN and EAB were supported by Imperial College Divisional Studentships.

Author contributions

J.L.V., G.A.R and M.M. designed research; J.L.V., T.J.N., E.A.B., M.S.K. conducted experiments, J.L.V., T.J.R., E.A.B, M.S.K., G.A.R. and M.M. analyzed data, and J.L.V., G.A.R. and M.M. wrote the paper.

Literature

1. B. L. Vallee et al., *Physiol. Rev.* **73** (1), 79-118 (1993).
2. N. C. Lim et al., *Chem. Eur. J.* **11** (1), 38 (2005).
3. W. Maret, *Biometals* **22** (1), 149-157 (2009).
4. D. W. Domaille et al., *Nat. Chem. Biol.* **4** (3), 168-175 (2008).
5. P. J. Dittmer et al., *J. Biol. Chem.* (2009) in press.
6. R. A. Bozym et al., *ACS Chem. Biol.* **1**, 103-111 (2006).
7. E. M. W. M. van Dongen et al., *J. Am. Chem. Soc.* **129** (12), 3494-3495 (2007).
8. J. L. Vinkenborg et al., *ChemBioChem* **8** (10), 1119-1121 (2007).
9. J.C. Hutton et al., *Biochem. J.* **210**, 297-305 (1983).
10. H.E. Hohmeier et al., *Diabetes* **49** (3), 424-430 (2000).
11. A. Krezel et al., *J. Biol. Inorg. Chem.* **11** (8), 1049-1062 (2006).
12. M. Taki et al., *J. Am. Chem. Soc.* **126** (3), 712-713 (2004).
13. K. J. Mitchell et al., *J. Cell Biol.* **155** (1), 41-51 (2001).
14. T. H. Evers et al., *J. Mol. Biol.* **374** (2), 411-425 (2007).
15. A. Krezel et al., *J. Am. Chem. Soc.* **129** (35), 10911-10921 (2007).

Figure 1

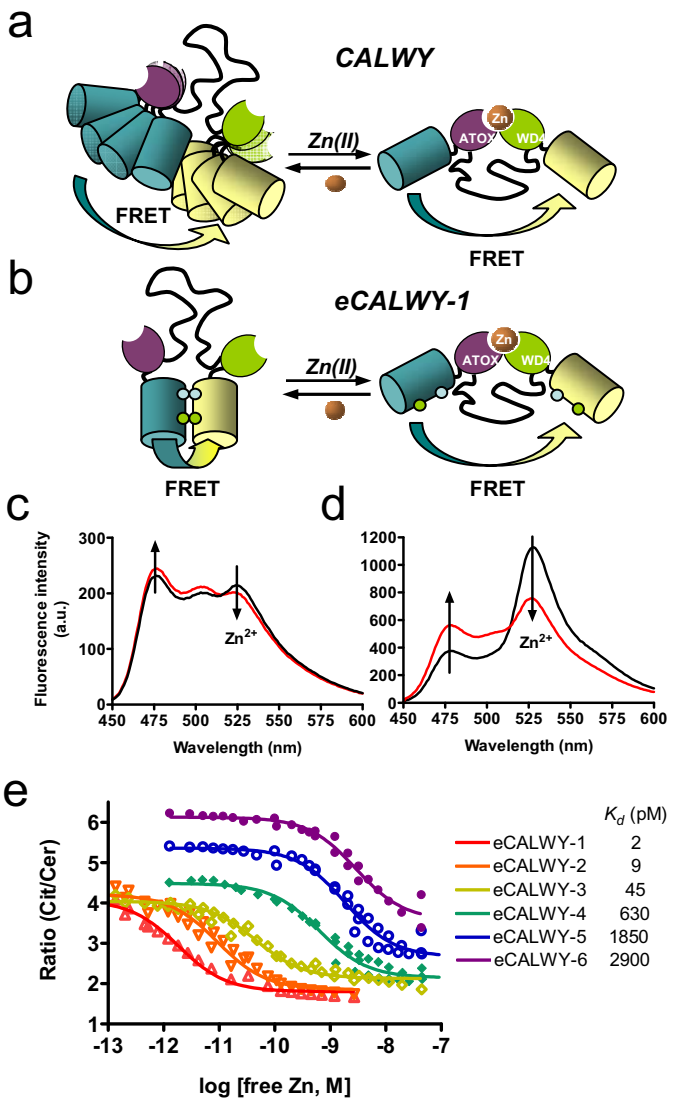
a
CALWY
Zn(II)
FRET
FRET
b
eCALWY-1
Zn(II)
FRET
FRET
c
d
Fluorescence intensity (a.u.)
Zn2+
Zn2+
Wavelength (nm)
Wavelength (nm)
e
Ratio (Cit/Cer)
log [free Zn, M]
Kd (pM)
eCALWY-1 2
eCALWY-2 9
eCALWY-3 45
eCALWY-4 630
eCALWY-5 1850
eCALWY-6 2900

Figure 2

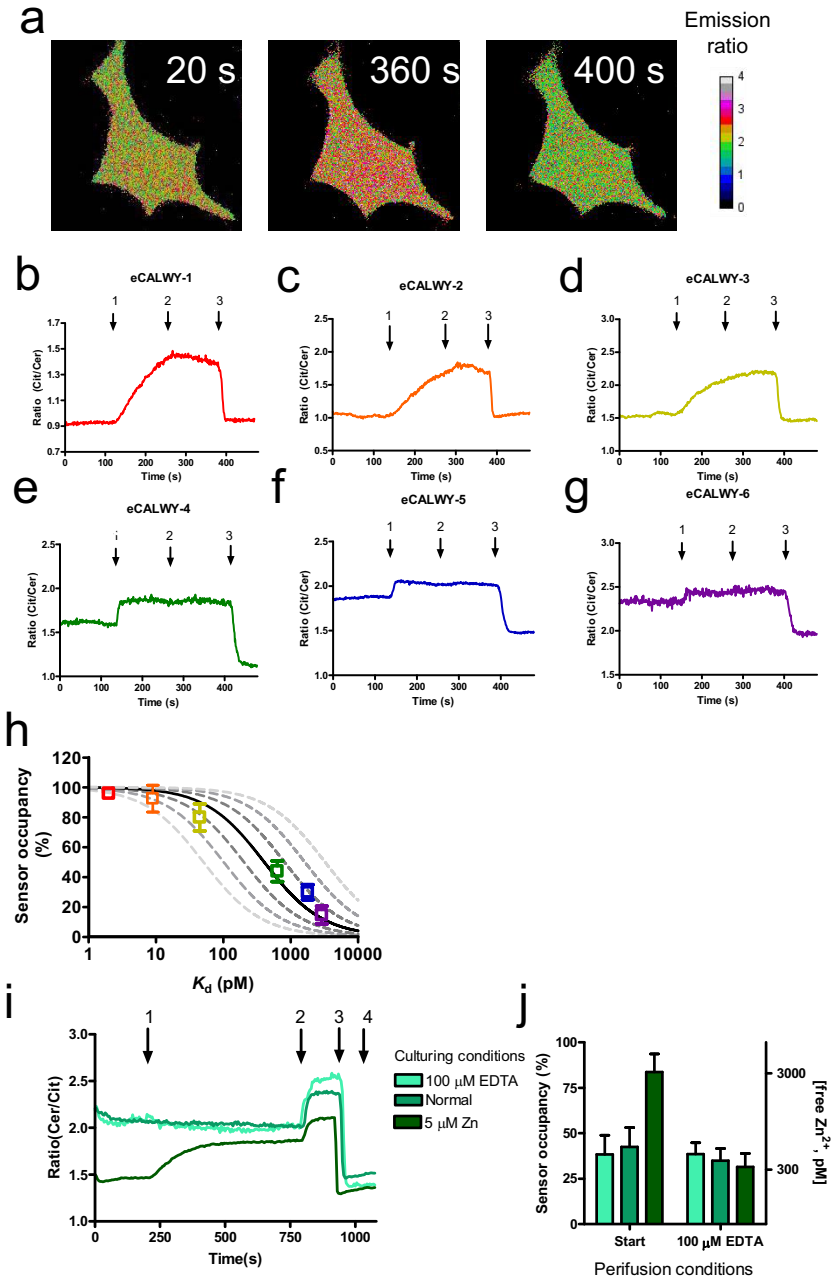
a
20 s
360 s
400 s
Emission ratio
4
3
2
1
0
b
eCALWY-1
c
eCALWY-2
d
eCALWY-3
e
eCALWY-4
f
eCALWY-5
g
eCALWY-6
Ratio (Cit/Cer)
Time (s)
h
Sensor occupancy (%)
K_d (pM)
i
Ratio(Cer/Cit)
Time(s)
Culturing conditions
100 μM EDTA
Normal
5 μM Zn
j
Sensor occupancy (%)
[free Zn^{2+}, pM]
Start
100 μM EDTA
Perifusion conditions

Figure 3

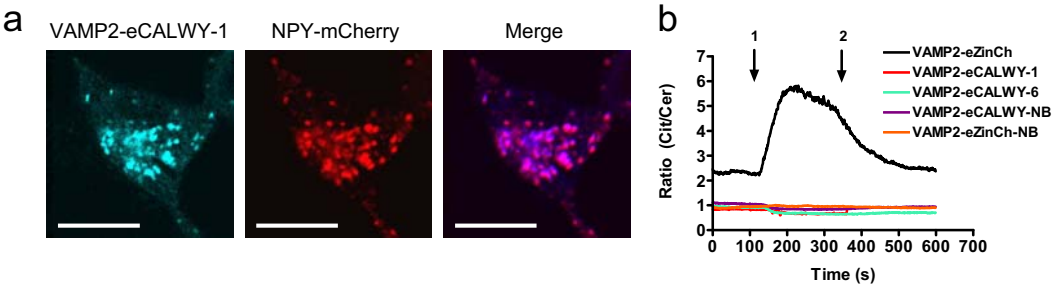
a
VAMP2-eCALWY-1
NPY-mCherry
Merge
b
1
2
VAMP2-eZinCh
VAMP2-eCALWY-1
VAMP2-eCALWY-6
VAMP2-eCALWY-NB
VAMP2-eZinCh-NB
Ratio (Cit/Cer)
0
1
2
3
4
5
6
7
0
100
200
300
400
500
600
700
Time (s)